

# FinPercep-RM: A Fine-grained Reward Model and Co-evolutionary Curriculum for RL-based Real-world Super-Resolution

Yidi Liu<sup>1,†</sup>, Zihao Fan<sup>1,†</sup>, Jie Huang<sup>1</sup>, Jie Xiao<sup>1</sup>, Dong Li<sup>1</sup>,  
**LEI BAI<sup>2</sup>, Xueyang Fu<sup>1,\*</sup>, Wenlong Zhang<sup>2,\*</sup>, Zheng-jun Zha<sup>1</sup>**

<sup>1</sup>University of Science and Technology of China <sup>2</sup>Shanghai AI Laboratory

liuyidi2023@mail.ustc.edu.cn, xyfu@ustc.edu.cn

\* Corresponding Author, † contributed equally.

## Abstract

*Reinforcement Learning with Human Feedback (RLHF) has proven effective in image generation field guided by reward models to align human preferences. Motivated by this, adapting RLHF for Image Super-Resolution (ISR) tasks has shown promise in optimizing perceptual quality with Image Quality Assessment (IQA) model as reward models. However, the traditional IQA model usually output a single global score, which are exceptionally insensitive to local and fine-grained distortions. This insensitivity allows ISR models to produce perceptually undesirable artifacts that yield spurious high scores, misaligning optimization objectives with perceptual quality and results in reward hacking. To address this, we propose a Fine-grained Perceptual Reward Model (FinPercep-RM) based on an Encoder-Decoder architecture. While providing a global quality score, it also generates a Perceptual Degradation Map that spatially localizes and quantifies local defects. We specifically introduce the FGR-30k dataset to train this model, consisting of diverse and subtle distortions from real-world super-resolution models. Despite the success of the FinPercep-RM model, its complexity introduces significant challenges in generator policy learning, leading to training instability. To address this, we propose a Co-evolutionary Curriculum Learning (CCL) mechanism, where both the reward model and the ISR model undergo synchronized curricula. The reward model progressively increases in complexity, while the ISR model starts with a simpler global reward for rapid convergence, gradually transitioning to the more complex model outputs. This easy-to-hard strategy enables stable training while suppressing reward hacking. Experiments validate the effectiveness of our method across ISR models in both global quality and local realism on RLHF methods.*

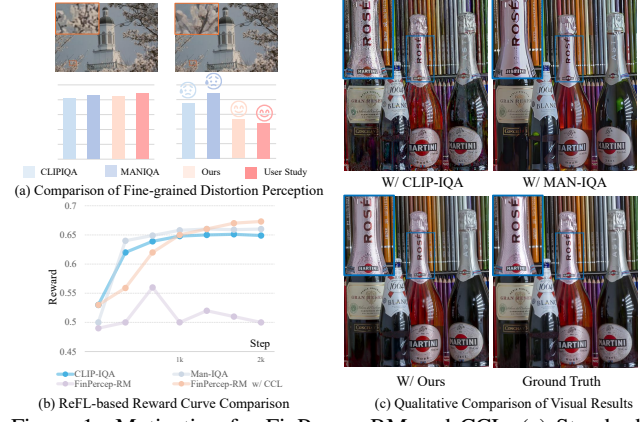


Figure 1. Motivation for FinPercep-RM and CCL. (a) Standard IQAs lack fine-grained perception and struggle to penalize local distortions, while Ours aligns with human judgment (User Study). (b) The training curves illustrate the stability-robustness dilemma: baseline IQA rewards (blue/purple) converge quickly, while FinPercep-RM (light blue) is oscillatory and unstable. Our complete method (FinPercep-RM w/ CCL, orange) achieves stable and optimal convergence. (c) Visualization of Reward Hacking: baseline rewards (W/ CLIP-IQA, W/ MAN-IQA) produce local artifacts, whereas ours results are faithful to the Ground Truth.

## 1. Introduction

Image Super-Resolution (ISR) [8, 29, 44, 51] aims to restore fine-grained details from low resolution images. Traditional ISR methods improve pixel-level fidelity but often produce overly smooth results lacking realistic details, especially in Real-world ISR (Real-ISR). Recently, generative methods [4, 5, 7, 9, 20, 30, 33, 42, 43, 46] leveraging large-scale pre-trained text-to-image (T2I) diffusion models have emerged as a promising solution for Real-ISR, which possess powerful generative priors to synthesize rich textures and achieve superior perceptual quality.

Meanwhile, Reinforcement Learning from Human Feedback (RLHF) has become a key optimization paradigm in

T2I [2, 18, 26, 37], and Reward Models (RMs) [16, 21, 35, 36, 49] have been widely explored to enhance visual aesthetics and alignment with user preferences. Therefore, migrating the RLHF to the Real-ISR task is desired to explore. Concretely, we aim to leverage RLHF to further refine the behavior of T2I priors within the SR context, guiding the model to generate restoration results with higher perceptual quality and fewer artifacts.

However, we find that typical reward models for ISR, i.e., Image Quality Assessment (IQA) models [11, 12, 14, 27, 38, 50], are not directly applicable to the specific challenges of Real-ISR that required fine-grained quality improvement. The core bottleneck is that traditional IQA models are dominated by global, coarse-grained perception, which easily brings a severe "Reward Hacking" problem for training ISR models with their generated reward signals. As illustrated in Fig. 1(a), standard IQAs (CLIP-IQA, MANIQA) lack fine-grained perception, failing to distinguish a subtly distorted image from its original and assigning both a similarly high score, in stark contrast to human evaluation. This pursuit of fallacious high rewards creates a critical misalignment. Consequently, as shown by the reward curves in Fig. 1(b), the generator quickly learns to "cater" to this inadequate reward signal. It successfully converges to a higher global reward score, but the resulting image exhibit obvious local artifacts and an unrealistic "painterly" appearance (see Fig. 1(c)). Although some large-scale IQA models [6, 23] demonstrate improved fine-grained perception, their utility as reward models for training is limited, as their perception is primarily semantic and their huge computational cost renders them impractical for iterative training on many devices.

In this paper, we propose a novel Fine-grained Perceptual Reward Model (FinPercep-RM) with a dedicated dataset termed FGR-30k for training RLHF of ISR. The core idea is that a robust RM should not only assess *What* the quality is, but also diagnose *Where* the defect is. Specifically, **1)** FinPercep-RM's is designed as an Encoder-Decoder architecture (see Fig. 2): the encoder based on a powerful IQA backbone generates a global quality score, while the decoder is trained to produce a fine-grained Perceptual Degradation Map(fg-PDM) that spatially localizes and quantifies local defects. **2)** FGR-30k dataset is constructed ISR's results from various Real-ISR models, covering a diverse range of real-world SR artifacts. As shown in Fig. 3, we synthesize a total of 30,000 fine-grained distortion samples by swapping regions between ISR's results and the ground-truth images using both random and semantic masks. We then combine two-level differences to construct a measure of the fine-grained quality discrepancy, which serves as the supervision signal for the above fg-PDM. Finally, our proposed FinPercep-RM demonstrates superior fine-grained perceptual capabilities (Fig. 1(a)), which en-

hances reward robustness and suppresses reward hacking.

Nevertheless, the FinPercep-RM often brings instability training in RLHF due to its spatially-complex property that increases policy learning difficulty, as shown in Fig. 1(b). This creates a dilemma between stability and robustness: a simple, low-variance global IQA reward is stable but prone to reward hacking, while the high-variance FinPercep-RM reward alleviates hacking but hinders convergence.

To further alleviate this FinPercep-RM training instability, we propose Co-evolutionary Curriculum Learning (CCL), which balance stability and robustness via two co-evolving paths (see Fig. 2): **1)** Reward Model Progressive Expansion: The RM training follows a curriculum, starting with a simple global IQA model and gradually introducing the decoder's parameters in stages as it trains on FGR-30k, evolving from a global score to a more complex model with a fine-grained heatmap. **2)** Generator Curriculum Co-evolution: The generator's RL training is synchronized with the RM evolution. Initially, it uses the global IQA reward for stable convergence, then progressively shifts to more complex FinPercep-RM versions, refining local details.

The dynamic training property of CCL enables end-to-end stability while leveraging the robust and fine-grained reward of FinPercep-RM in the later stages to achieve meticulous optimization of local perceptual quality. In summary, our contributions are listed as follows:

- We are the first to attribute the RLHF benefit bottleneck in Real-ISR to the insufficient fine-grained perceptual capability of the reward model. We design FinPercep-RM, a diagnostic reward model capable of identifying local defects via fine-grained Perceptual Degradation Maps, alleviating the reward hacking in RL-based Real-ISR.
- We construct the FGR-30k dataset, which builds supervision signals for FinPercep-RM by combining pixel and feature differences, providing a data foundation for training diagnostic reward models.
- We devise the CCL mechanism, which alleviates the conflict between training stability and reward robustness by co-evolving curricula of the reward model and ISR model.

## 2. Related Work

### 2.1. Real-World Image Super-Resolution

Image Super-Resolution (ISR) has been extensively studied [8, 29, 44, 51]. However, these methods often produce overly smooth results lacking realistic details, especially in real-world scenarios where degradations are complex and unknown. Recent diffusion model-based approaches [4, 5, 7, 9, 20, 30, 33, 42, 43, 46] for Real-World ISR have made remarkable progress. These methods exploit the powerful generative priors embedded in pre-trained text-to-image (T2I) diffusion models to tackle Real-ISR tasks, StableSR [28] injects LR information into stable

diffusion models via ControlNet[45], significantly improving fidelity under real-world degradations. DiffBIR[17] and PASD[39] first employ degradation-restoration modules to reduce degradations, and then enhance details through conditional branches to guide the diffusion process. At the semantic level, SeeSR[34], CoSeR[24] and PiSA-SR[25] further introduce language–vision collaboration mechanisms, leveraging text semantics and pixel representations to enable multi-scale, controllable diffusion. SUPIR[40] and Dreamclear[1] show that scaling model and data size significantly enhances photorealistic performance. The recent DiT4SR[10] introduces the Diffusion Transformer (DiT) architecture[19] to the SR task, incorporating an LR stream into the original DiT block and laying the foundation for future large-scale diffusion-based SR models.

## 2.2. Reward Models and Image Quality Assessment

Traditional image quality assessment (IQA) methods are generally divided into full-reference (FR) [31, 47] and no-reference (NR) [14, 27, 38, 50] approaches, depending on whether a ground-truth reference image is available. Early assessments of text-to-image (T2I) diffusion models mainly relied on metrics such as FID[12] and CLIPScore[11]. Recently, reward models have emerged to align quality assessment with human preferences like Aesthetic Predictor[21], ImageReward[36], PickScore[16], MPS[49] and HPSv2[35] which enhance preference alignment through larger and more diverse datasets. Nevertheless, these models produce only a single global score, overlooking spatial and semantic variations crucial for fine-grained perception. This limitation motivates our FinPercep-RM, which enables localized and perceptually aligned evaluation for Real-ISR tasks.

## 3. Method

### 3.1. Overview

We propose an RL optimization framework to resolve the inherent challenges of *Reward Hacking* and *Training Instability* when applying RLHF to Real-ISR tasks. As illustrated in Fig. 2, the framework comprises three core components:(1) The Generator, a T2I-prior-based Real-ISR model tasked with generating  $I_{SR}$ ; (2) The Diagnostic Reward Model (FinPercep-RM, Sec. 3.2), which assesses the fine-grained perceptual quality of  $I_{SR}$ ; and (3) The Co-evolutionary Curriculum Learning (CCL) Mechanism (Sec. 3.5), which modulates the training process to balance stability and robustness.

During the RL inner loop (at stage  $k$ ), the Generator generates  $I_{SR}$ . The corresponding reward model,  $RM_k$  (a specific version of FinPercep-RM), evaluates it along two dimensions: "What" (a global score  $S_{global}$ ) and "Where" (a local degradation map  $M_{pdm}$ ). These outputs are fused into

a scalar reward  $R_k$ , which guides the Generator's policy update to optimize perceptual quality.

To prevent the instability caused by a strict RM, the CCL mechanism introduces an "outer loop" that co-evolves both components. The RM progressively expands from a simple global IQA model ( $RM_0$ ) to a complex fine-grained model( $RM_N$ ) by training on FGR-30k (Sec. 3.3). Simultaneously, the Generator's curriculum co-evolves, starting with the stable  $RM_0$  and migrating to stricter  $RM_k$  versions. This easy-to-hard dynamic matching promotes early-stage stability while suppressing late-stage reward hacking via robust, fine-grained rewards.

### 3.2. The architecture of FinPercep-RM

To mitigate the vulnerability of coarse global rewards to reward hacking in Real-ISR, we introduce the Fine-grained Perceptual Reward Model (FinPercep-RM), as shown in the top of Fig. 2. The central hypothesis is that reward hacking stems from the RM's failure to perceive localized spatial defects. Our core idea is to architecturally couple the global quality score (the What) with a fine-grained defect map (the Where). This coupling ensures the global score is innately sensitive to local imperfections. Specifically, given a generator  $G_\theta$  that produces  $I_{SR} = G_\theta(I_{LR}, z)$  (where  $z$  denotes sampled noise/latent), FinPercep-RM  $RM_\phi$  returns a pair of complementary signals:

$$\{S_{fgc\text{-global}}, M_{fg\text{-pdm}}\} = RM_\phi(I_{SR}), \quad (1)$$

where Fine-grained Calibrated Global score  $S_{fgc\text{-global}}$  approximates human-perceived global quality, and Fine-grained Perceptual Degradation Map (Fg-PDM)  $M_{fg\text{-pdm}}$  measures the spatial likelihood and intensity of local defects; where larger values indicate a higher probability of unrealistic textures or artifacts.

To achieve this goal, FinPercep-RM adopts an encoder–decoder paradigm, as shown in Fig 2.

**Encoder:** We utilize a classical IQA backbone (e.g., CLIP-IQA) as the encoder  $E$ . The encoder takes  $I_{SR}$  as input and extracts multi-scale representations  $\{f_i\}_{i=1}^N$ . These feature maps contain both high-level semantics (for global assessment) and low-level spatial details (for defect localization). We denote  $f_N$  as the deepest representation, i.e., the final global feature map.

**Decoder and PDM ( $M_{fg\text{-pdm}}$ ):** The decoder  $D$  receives the multi-scale representations  $\{f_i\}_{i=1}^N$ . Through a series of up-sampling and cross-layer fusion operations, the decoder reconstructs a Perceptual Degradation Map at the same resolution as  $I_{SR}$ . This map is normalized via a Sigmoid activation to produce  $M_{fg\text{-pdm}} \in [0, 1]$ .

**Fine-grained Calibrated Global score ( $S_{fgc\text{-global}}$ ):** A key architectural innovation is the formulation of  $S_{fgc\text{-global}}$ . Rather than regressing a score directly from  $f_N$ , our objective is to make this score explicitly dependent on the

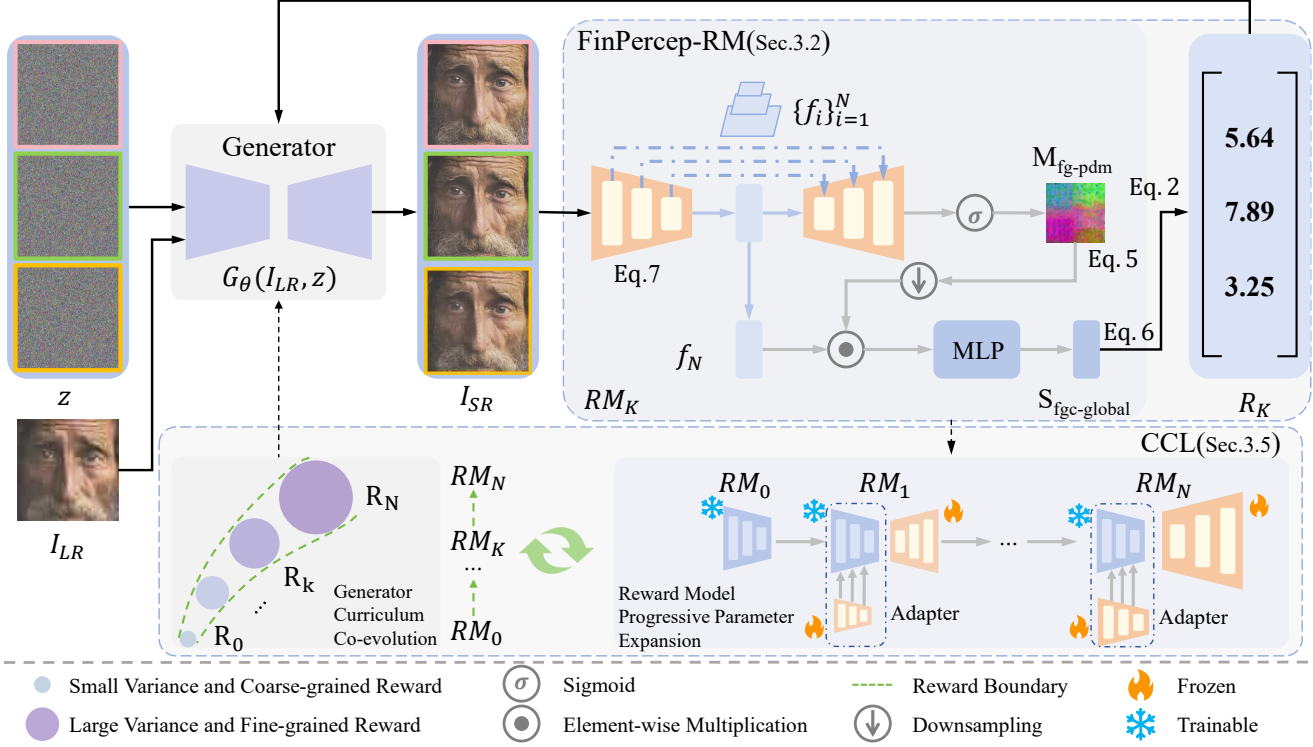


Figure 2. The overall pipeline of the proposed FinPercep-RM and Co-evolutionary Curriculum Learning (CCL) framework. FinPercep-RM produces a Fine-grained Perceptual Degradation Map that captures spatially localized defect likelihood and intensity, and the reward model is progressively expanded from small-variance, coarse-grained rewards to large-variance, fine-grained signals. During training, under the CCL mechanism, the Generator first learns with the coarse global reward from  $RM_0$  for a stable and easy initialization, and is then co-evolutionarily guided by increasingly strict  $RM_k$  versions to enhance local fidelity and suppress reward hacking.

$M_{\text{fg-pdm}}$ . To achieve this, we modulate the deepest global representation  $f_N$  using the interpolated defect map  $M_{\text{pdm}}$ . This operation compels the model to account for spatial defects when calculating the final score. The modulated feature is then passed to an MLP head to regress the scalar score  $S_{\text{fgc-global}}$ .

$$\begin{aligned} \{f_i\}_{i=1}^N &= \text{Encoder}(I_{\text{SR}}) \\ M_{\text{fg-pdm}} &= \text{Sigmoid}(\text{Decoder}(\{f_i\}_{i=1}^N)) \\ S_{\text{fgc-global}} &= \text{MLP}(f_N \odot \text{interpolate}(M_{\text{pdm}})), \end{aligned} \quad (2)$$

where  $\text{interpolate}(\cdot)$  denotes bilinear interpolation,  $\text{Sigmoid}(\cdot)$  denotes sigmoid activation function, and  $\odot$  denotes element-wise multiplication.

### 3.3. FGR-30k: A Fine-grained Reward Dataset

The training of FinPercep-RM, particularly its decoder  $D$ 's ability to reconstruct  $M_{\text{fg-pdm}}$ , requires high-quality supervision data with spatial defect annotations. Existing IQA and preference datasets (e.g., Aesthetic, Pick-a-Pic) lack this. To fill this gap, we built FGR-30k, a 30,000-sample fine-grained reward dataset for Real-ISR. The dataset provides  $(I_{\text{syn}}, M_{\text{gt}})$  pairs (a distorted sample and its ground-truth

map) to supervise FinPercep-RM. Construction involves two steps: synthesizing distortion samples and generating their ground-truth PDMs. Our data construction pipeline is illustrated in Fig. 3.

#### 3.3.1. Synthesis of Fine-grained Distortion Samples

To acquire a diverse and realistic source of artifacts, our data construction pipeline begins by collecting high-quality, real-world images  $I_{\text{GT}}$  from the internet, covering a wide range of scenes. Next, we employ the degradation pipeline from Real-ESRGAN [29] to apply complex, realistic degradations to each  $I_{\text{GT}}$ , generating corresponding low-resolution images  $I_{\text{LR}}$ . Finally, we feed  $I_{\text{LR}}$  into Diffusion base SR model pool (including multiple open-source Real-ISR models) to generate the sr results  $I_{\text{SR}}$ . This process provides us with a rich and authentic source of artifacts.

However,  $I_{\text{SR}}$  samples contain global, not localized, degradation. To create precise training data, we employ a **Region Swapping** strategy to synthesize  $I_{\text{syn}}$ . This method controllably "implants" local defects by swapping regions between  $I_{\text{GT}}$  (high-quality) and  $I_{\text{SR}}$  (artifact-laden). We use two mask types  $M$ : (1) **Random Masks** (rectangular/free-form) to identify blocky or non-semantic artifacts, and (2)

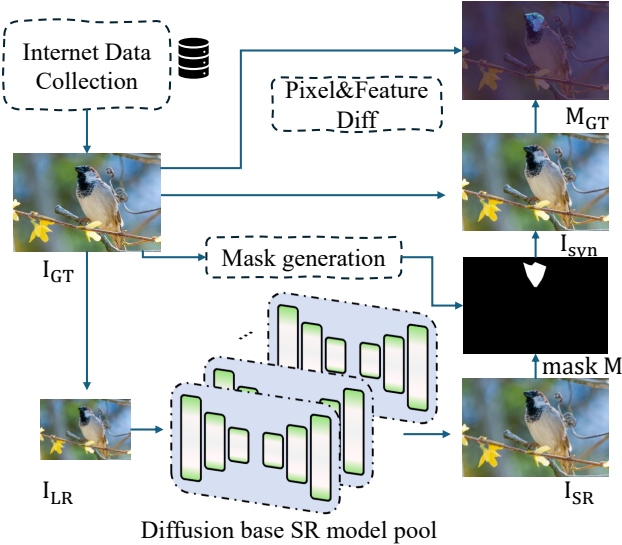


Figure 3. FGR-30k construction pipeline. We synthesize fine-grained distortion samples by swapping artifact-rich regions from diffusion-based SR outputs into clean images, using both random and semantic masks. Ground-truth perceptual degradation maps are generated by fusing pixel- and feature-level dissimilarities (via DINOv3), providing spatially precise supervision for training FinPercep-RM.

**Semantic Masks** (from SAM [15]) to synthesize realistic, object-based degradations. The synthesis, formulated as:

$$I_{\text{syn}} = M \odot I_{\text{SR}} + (1 - M) \odot I_{\text{GT}} \quad (3)$$

Using this method, we generated 30,000  $I_{\text{syn}}$  samples, each containing localized artifacts sourced from real SR models.

### 3.3.2. Ground-Truth PDM Generation

The generation of a corresponding ground-truth map  $M_{\text{gt}}$  for each synthesized sample  $I_{\text{syn}}$  is essential for supervision. To ensure  $M_{\text{gt}}$  accurately quantifies the fine-grained perceptual discrepancy, it is formulated as a composite of low-level pixel and high-level feature dissimilarities. (1)

**Pixel-level Dissimilarity (Diff<sub>pixel</sub>):** We compute the  $L_1$  distance map ( $|I_{\text{syn}} - I_{\text{GT}}|$ ) to capture fundamental chromatic and luminance deviations. (2) **Feature-level Dissimilarity (Diff<sub>feat</sub>):** To identify more complex misalignments, we compute the spatial Cosine Distance between deep feature embeddings,  $f_{\text{syn}}$  and  $f_{\text{GT}}$ , extracted via a pre-trained DINOv3 model [22]. This captures high-level structural, textural, and semantic inconsistencies.

The final ground-truth  $M_{\text{gt}}$  is a weighted fusion of these two differences, followed by normalization:

$$\begin{aligned} \text{Diff}_{\text{pixel}} &= |I_{\text{syn}} - I_{\text{GT}}|; \text{Diff}_{\text{feat}} = 1 - \cos(f_{\text{syn}}, f_{\text{GT}}) \\ M_{\text{gt}} &= \text{Normalize}(\alpha \cdot \text{Diff}_{\text{pixel}} + (1 - \alpha) \cdot \text{Diff}_{\text{feat}}) \end{aligned} \quad (4)$$

where  $\alpha$  is a balancing hyperparameter. This resulting  $M_{\text{gt}}$  is sensitive not only to local artifacts but also to se-

mantically misaligned structures, providing a robust and information-rich supervision signal for FinPercep-RM.

### 3.4. Training FinPercep-RM with FGR-30k

To train FinPercep-RM’s global and diagnostic capabilities, we sample  $(I_{\text{GT}}, I_{\text{syn}}, M_{\text{gt}})$  pairs from FGR-30k. Our total objective  $\mathcal{L}_{\text{total}}$  combines three components: a dense heatmap loss ( $\mathcal{L}_{\text{map}}$ ) for  $M_{\text{fg-pdm}}$ , a triplet ranking loss ( $\mathcal{L}_{\text{rank}}$ ) for  $S_{\text{fgc-global}}$ , and an anchor alignment loss ( $\mathcal{L}_{\text{align}}$ ) to stabilize the score scale.

For the dense heatmap loss  $\mathcal{L}_{\text{map}}$ , we use L1 loss to supervise the predicted  $M_{\text{fg-pdm}}$  and the ground-truth  $M_{\text{gt}}$ , represented as:

$$\mathcal{L}_{\text{map}} = \mathbb{E}_{(I_{\text{syn}}, M_{\text{gt}}) \sim \text{FGR-30k}} \|M_{\text{fg-pdm}} - M_{\text{gt}}\|_1, \quad (5)$$

where  $\|\cdot\|_1$  denotes the L1 norm.

For the triplet ranking loss, first, given the triplet  $\{I_{\text{SR}}, I_{\text{syn}}, I_{\text{GT}}\}$ , the model computes their respective scores  $S_{\text{SR}}$ ,  $S_{\text{syn}}$ , and  $S_{\text{GT}}$ . Since  $I_{\text{syn}}$  originates from a partial region swap between  $I_{\text{GT}}$  and  $I_{\text{SR}}$ , the triplet ranking loss is consequently defined as follows:

$$\begin{aligned} \mathcal{L}_{\text{rank}} = \mathbb{E} [ & \max(0, m_1 - (S_{\text{fgc-global}} - S_{\text{SR}})) \\ & + \max(0, m_2 - (S_{\text{GT}} - S_{\text{fgc-global}})) ], \end{aligned} \quad (6)$$

where  $\max(0, \cdot)$  denotes the hinge loss,  $m_1$  and  $m_2$  are the margin parameters. This loss ensures that  $S_{\text{fgc-global}}$  is ranked higher than  $S_{\text{SR}}$  and lower than  $S_{\text{GT}}$ .

The ranking loss solely guarantees the relative order of the scores, not their absolute scale. This can lead to ‘score drifting’ across different training stages (particularly during the CCL process), rendering the rewards from different stages incomparable. To address this issue, we further introduce an anchor alignment loss,  $\mathcal{L}_{\text{align}}$ , to align the absolute score for  $I_{\text{GT}}$  between our current FinPercep-RM and the original pre-trained IQA model. This loss is formulated as follows:

$$\mathcal{L}_{\text{align}} = \mathbb{E}_{(I_{\text{GT}}) \sim \text{FGR-30k}} \|S(I_{\text{GT}}) - S_{\text{base}}(I_{\text{GT}})\|_1 \quad (7)$$

where  $S_{\text{base}}(\cdot)$  represents the score output of the original pre-trained IQA model.

Finally, the total training loss for FinPercep-RM is a weighted sum of the three preceding losses:

$$\mathcal{L}_{\text{total}} = \lambda_{\text{map}} \cdot \mathcal{L}_{\text{map}} + \lambda_{\text{rank}} \cdot \mathcal{L}_{\text{rank}} + \lambda_{\text{align}} \cdot \mathcal{L}_{\text{align}}, \quad (8)$$

where  $\lambda_{\text{map}}$ ,  $\lambda_{\text{rank}}$ , and  $\lambda_{\text{align}}$  are hyperparameters used to balance the importance of each task. Through this combination, FinPercep-RM becomes a robust reward model capable of both precisely localizing defects and providing global scores enhanced by fine-grained perception.

### 3.5. Integrating FinPercep-RM for ISR with CCL

While FinPercep-RM resolves reward hacking via fine-grained diagnostics, its non-smooth reward signal introduces a severe training stability challenge. We observe that directly using the complete FinPercep-RM from the outset creates a difficult exploration space, where minor local penalties cause policy gradient oscillations and potential convergence failure (Fig. 1(b)).

This presents a dilemma: *simple global IQA rewards are stable but converge to a suboptimal hacked solution, whereas the robust FinPercep-RM ensures a correct objective but compromises training stability.* To improve this stability-robustness trade-off, we propose Co-evolutionary Curriculum Learning (CCL) in Fig. 2, which co-evolves the RM and the generator ( $G_\theta$ ), prioritizing stability in early stages and progressively shifting to robustness.

#### 3.5.1. Reward Model Progressive Parameter Expansion

The first CCL path involves the progressive evolution of the RM. We construct a sequence of models,  $\{RM_0, RM_1, \dots, RM_N\}$ , with increasing diagnostic capability and complexity via staged training on the FGR-30k dataset. This curriculum begins with a baseline global IQA model,  $RM_0$  (e.g., a pre-trained CLIP-IQA), which provides a smooth, stable reward for initial convergence. In the next stage ( $k = 1$ ), we attach the lightweight decoder  $D$  (Sec. 3.2) to form  $RM_1$ , which begins training on FGR-30k to acquire preliminary diagnostic capabilities, enabling it to output  $(M_{\text{fg-pdm}}, S_{\text{fgc-global}})$ . In subsequent stages ( $k > 1$ ), we progressively scale the parameter counts of both the decoder  $D$  and Adapter modules inserted into the encoder  $E$ . This progressive parameter growth ensures a smooth evolution from the basic  $RM_1$  to the  $RM_N$  with complete fine-grained perceptual capabilities, avoiding training instability caused by abrupt changes in model capacity.

#### 3.5.2. Generator Curriculum Co-evolution

The second CCL path involves matching the generator’s ( $G_\theta$ ) training curriculum to the RM’s evolution, ensuring an appropriately difficult reward environment at each stage  $k$ . In the initial training stage ( $k = 0$ ),  $G_\theta$  trains using only the stable global reward from  $RM_0$ . This smooth and stable reward signal allows the generator’s policy  $\pi_\theta$  to quickly converge to a correct general direction, thereby establishing a robust initial policy. Subsequently, as the curriculum advances and the training stage  $k$  gradually increases, the environment is switched to the more robust reward model  $RM_k$ . The generator then refines its policy under this more sensitive reward signal. This easy-to-hard, dynamically matched co-evolutionary paradigm deftly balances stability and robustness. The generator achieves rapid, stable convergence in the early stages using simple rewards. In the later stages, by learning from the increasingly capable RM

sequence, it progressively refines local texture details and effectively suppresses artifact generation, ultimately ensuring stable convergence while preventing reward hacking.

For the specific policy optimization, we validate the effectiveness of our reward model using REFL [36], DPO [26], and GRPO [37]. During stage  $k$  of the CCL, the generator’s policy  $\pi_\theta$  is updated based on the reward signal  $R_k$  (derived from the  $S_{\text{fgc-global}}$  output at the current stage).

## 4. Experiments

**Baseline:** FinPercep-RM is trained and extended based on the pretrained CLIP-IQA [27]. We evaluate our proposed FinPercep-RM on three real-world super-resolution baselines: DiffBIR [17], SeeSR [34], and DIT4SR [10], and conduct **RLHF by Reward feedback learning (REFL)** [36] using the reward signals provided by FinPercep-RM. To verify the performance improvements brought by FinPercep-RM, we compare with variants that directly use **CLIP-IQA** as the reward model.

**Datasets:** Both the training and validation datasets follow the paradigm established in DIT4SR [10]. The real-world super-resolution capacity of the models is assessed on four widely adopted real datasets: DrealSR [32], RealSR [3], RealLR200 [34], and RealLQ250 [1]. All experiments are conducted under a 4 $\times$  upscaling setting.

**Evaluation Metrics:** In line with previous works in real-world super-resolution [1, 10, 13, 41], PSNR and SSIM [31] are inadequate for measuring perceptual differences. Therefore, we employ LPIPS [48] to quantify image fidelity and use four no-reference metrics—MUSIQ [14], MANIQA [38], ClipIQA [27], and LIQE [50] to evaluate perceptual quality. In addition, we conduct a user study to comprehensively assess both fidelity and perceptual quality.

### 4.1. Comparison with Other Methods

As shown in Tab. 1, our approach achieves superior quantitative results across four real-world benchmarks. Specifically, incorporating FinPercep-RM with all three baseline models (DiffBIR, SeeSR, and DIT4SR) consistently leads to the best performance on nearly all perceptual metrics (MUSIQ, MANIQA, LIQE), while also markedly reducing LPIPS distortion compared to both the original baselines and other state-of-the-art methods.

Meanwhile, directly using the original CLIP-IQA as the reward signal for RLHF fine-tuning (“w/ IQA”) often leads to severe “reward hacking” issues: although the performance improves on the CLIP-IQA metric itself, most other perceptual quality metrics show clear deterioration. This demonstrates that our FinPercep-RM, by leveraging its fine-grained perception capacity, delivers a more robust and accurate reward signal. As a result, it not only successfully guides generators to enhance perceptual quality but

Datasets	Metrics	ResShift			SUPIR			DreamClear			DiffBIR			SeeSR			DIT4SR		
		Baseline	w/ IQA	w/ Ours	Baseline	w/ IQA	w/ Ours	Baseline	w/ IQA	w/ Ours	Baseline	w/ IQA	w/ Ours	Baseline	w/ IQA	w/ Ours	Baseline	w/ IQA	w/ Ours
DrealSR	LPIPS $\downarrow$	0.353	0.419	0.354	0.452	0.465	0.428	0.317	0.332	0.295	0.365	0.378	0.342	0.319	0.332	0.302	0.365	0.378	0.342
	MUSIQ $\uparrow$	52.392	59.744	44.047	65.665	64.892	67.234	65.077	64.123	67.891	64.950	63.456	67.823	68.073	66.789	70.891	68.073	66.789	70.891
	MANIQA $\uparrow$	0.476	0.552	0.455	0.629	0.612	0.648	0.605	0.591	0.632	0.627	0.608	0.651	0.661	0.642	0.678	0.661	0.642	0.678
	ClipIQA $\uparrow$	0.379	0.518	0.379	0.572	0.589	0.586	0.543	0.567	0.561	0.548	0.562	0.574	0.550	0.596	0.598	0.550	0.596	0.598
	LIQE $\uparrow$	2.798	3.728	2.401	3.894	3.756	4.089	4.126	3.987	4.234	3.964	3.812	4.187	3.977	3.856	4.289	3.977	3.856	4.289
RealSR	LPIPS $\downarrow$	0.316	0.357	0.325	0.347	0.361	0.328	0.299	0.314	0.281	0.319	0.332	0.302	0.319	0.332	0.302	0.319	0.332	0.302
	MUSIQ $\uparrow$	56.892	61.929	59.396	68.340	67.123	70.156	69.675	68.234	71.234	68.073	66.789	70.891	68.073	66.789	70.891	68.073	66.789	70.891
	MANIQA $\uparrow$	0.511	0.574	0.546	0.653	0.634	0.672	0.643	0.628	0.669	0.661	0.642	0.678	0.661	0.642	0.678	0.661	0.642	0.678
	ClipIQA $\uparrow$	0.452	0.524	0.546	0.586	0.592	0.596	0.577	0.584	0.582	0.550	0.596	0.598	0.550	0.596	0.598	0.550	0.596	0.598
	LIQE $\uparrow$	2.853	3.780	3.221	4.026	3.912	4.234	4.123	4.001	4.345	3.977	3.856	4.289	3.977	3.856	4.289	3.977	3.856	4.289
RealLR200	MUSIQ $\uparrow$	59.695	64.837	65.926	68.027	66.789	70.234	69.428	68.456	71.567	70.469	69.123	72.234	70.469	69.123	72.234	70.469	69.123	72.234
	MANIQA $\uparrow$	0.525	0.600	0.597	0.629	0.612	0.656	0.612	0.598	0.645	0.645	0.628	0.662	0.645	0.628	0.662	0.645	0.628	0.662
	ClipIQA $\uparrow$	0.452	0.524	0.546	0.582	0.598	0.589	0.566	0.572	0.579	0.588	0.598	0.598	0.588	0.608	0.598	0.588	0.608	0.598
	LIQE $\uparrow$	3.054	3.626	3.775	4.003	3.889	4.234	4.006	3.912	4.345	4.331	4.123	4.456	4.331	4.123	4.456	4.331	4.123	4.456
RealLQ250	MUSIQ $\uparrow$	59.337	66.016	66.693	69.876	68.567	72.123	70.556	69.234	72.789	71.832	70.456	73.456	71.832	70.456	73.456	71.832	70.456	73.456
	MANIQA $\uparrow$	0.500	0.584	0.585	0.624	0.607	0.651	0.594	0.580	0.638	0.632	0.615	0.658	0.632	0.615	0.658	0.632	0.615	0.658
	ClipIQA $\uparrow$	0.417	0.483	0.502	0.578	0.592	0.585	0.562	0.579	0.571	0.578	0.583	0.586	0.578	0.583	0.586	0.578	0.583	0.586
	LIQE $\uparrow$	2.753	3.605	3.688	4.003	3.889	4.345	4.005	3.912	4.456	4.356	4.234	4.567	4.356	4.234	4.567	4.356	4.234	4.567

Table 1. Quantitative results of Real-ISR methods on four real-world benchmarks based on RLHF method of REFL [36]. Best and second best results are highlighted in red and blue, respectively. w/Ours achieves the best or comparable performance across four benchmarks.



Figure 4. Qualitative comparisons with state-of-the-art Real-ISR methods on on RealSR based on RLHF method of REFL [36].

Ours vs.	DIT4SR	SeeSR	DiffBIR	DreamClear
Realism	78.9%	85.3%	84.2%	76.4%
Fidelity	76.8%	72.6%	80.1%	74.2%

Table 2. User study results on real-world datasets. The percentages denote the frequency with which DIT4SR w/Ours was preferred over each compared approach, for both realism and fidelity.

Metrics	CLIP-IQA			Ours		
	DPO	GRPO	REFL	DPO	GRPO	REFL
MUSIQ $\uparrow$	69.234	68.567	70.456	<b>72.789</b>	72.123	<b>73.456</b>
MANIQA $\uparrow$	0.608	0.602	0.615	<b>0.651</b>	0.645	<b>0.658</b>
ClipIQA $\uparrow$	<b>0.591</b>	0.589	0.583	0.585	0.584	0.586
LIQE $\uparrow$	4.123	4.056	4.234	<b>4.456</b>	4.389	<b>4.567</b>

Table 3. Comparison of training strategies under IQA guidance vs. our method. Higher is better for all metrics.

Model	DINO	Coupled	CCL	MUSIQ $\uparrow$	MANIQA $\uparrow$
	loss	RM	Type		
FULL	✓	✓	Param	73.456	0.658
A	✗	✓	Param	72.123	0.638
B	✓	✗	Param	72.328	0.650
C	✓	✓	✗	71.982	0.645
D	✓	✓	Weight	72.842	0.648

Table 4. Ablation results on RealLQ250 for our DiT4SR. All variants are trained using the same settings as the full model.

also suppresses distortion, thus effectively preventing reward hacking.

As shown in Fig. 4, after applying FinPercep-RM (using REFL) to the three baselines, all models generate significantly improved visual results with enhanced details while effectively suppressing artifacts. Additional visual results are provided in the supp. Furthermore, to comprehensively compare our method against others in terms of both fidelity and realism, we conducted a user study, as shown in Tab. 2. The results demonstrate that ours significantly outperforms all other methods in both fidelity and realism.

#### 4.2. Effectiveness of Different RLHF Strategies

To demonstrate that our FinPercep-RM serves as a superior reward signal independent of specific RLHF algorithms, we systematically compared three popular RLHF alignment strategies: REFL [36], DPO [26], and GRPO [37]. For each approach, we conducted experiments on the DIT4SR model using both the standard CLIP-IQA and our FinPercep-RM as reward functions. As summarized in Table 3, when CLIP-IQA is adopted as the reward, all three RLHF strategies fail to improve model performance on RealLQ250 and may even degrade it, highlighting persistent reward hacking issues. In sharp contrast, replacing CLIP-IQA with our FinPercep-RM as the reward consistently leads to significant improvements across all three RLHF strategies. This

indicates that FinPercep-RM delivers stable and meaningful optimization signals that can be effectively leveraged by diverse RLHF algorithms. Overall, these results strongly validate that our FinPercep-RM is a more robust and effective reward function, whose advantages are not tied to any single RLHF alignment strategy.

#### 4.3. Ablation Study

We conducted a comprehensive ablation study on the proposed FinPercep-RM and CCL training strategies; detailed results are provided in Tab. 4. First, we analyzed the  $M_{fg\text{-}pdm}$  construction. Relying solely on pixel-wise differences (Variant A) caused a significant performance drop, highlighting that feature-level differences are crucial for enhancing generalization and preventing pixel-level overfitting. Next, we decoupled the fusion between the encoder output  $f_N$  and decoder output  $M_{fg\text{-}pdm}$  in FinPercep-RM, using a simple weighted combination of the encoder-derived global score  $S_{\text{global}}$  and  $M_{fg\text{-}pdm}$  to compute the reward signal  $R_k = \lambda_1 S_{\text{global}} + \lambda_2 (1 - \max(M_{fg\text{-}pdm}))$  (variant B). This also led to performance degradation, further verifying that fine-grained perception is beneficial for optimizing the overall score. Finally, we examined different CCL designs: "Param" denotes the default parameter-incremental CCL, and "Weight" means the parameter size of FinPercep-RM is fixed while the weights of fine-grained perception-related losses  $\mathcal{L}_{\text{map}}$  and  $\mathcal{L}_{\text{rank}}$  are progressively increased during training. Experimental results (variants C and D) show that removing CCL exposes the generator to high-variance rewards in early training, making convergence difficult; while gradually increasing loss weights can improve stability to some extent, it still does not match the overall efficacy of the parameter-incremental CCL. These results fully validate the critical roles of each module design in enabling both strong performance and training stability.

### 5. Conclusion

In this work, we addressed the critical challenges of *Reward Hacking* and *Training Instability* in T2I-prior-based Real-ISR. We identified the root cause of reward hacking as the lack of fine-grained perception in existing IQA models. To resolve this, we proposed FinPercep-RM, a diagnostic reward model that assesses both global quality ("What") and local defects ("Where"), trained on our newly constructed FGR-30k dataset which provides 30,000 samples with localized, synthesized artifacts. While FinPercep-RM effectively prevents hacking, its signal complexity introduces training instability. We therefore introduced the Co-evolutionary Curriculum Learning (CCL) mechanism to resolve this stability-robustness dilemma. CCL employs an easy-to-hard strategy that co-evolves both models: the RM progressively expands from a simple, global-only encoder ( $RM_0$ ) to the full-capacity  $RM_N$ , while the generator trains

first on  $RM_0$  for stable convergence before migrating to the stricter  $RM_k$  sequence to refine local details. This co-evolutionary paradigm successfully balances training stability with fine-grained reward robustness, ultimately preventing reward hacking and achieving state-of-the-art perceptual quality.

## References

- [1] Yuang Ai, Xiaoqiang Zhou, Huaibo Huang, Xiaotian Han, Zhengyu Chen, Quanzeng You, and Hongxia Yang. Dream-clear: high-capacity real-world image restoration with privacy-safe dataset curation. In *Proceedings of the 38th International Conference on Neural Information Processing Systems*, Red Hook, NY, USA, 2024. Curran Associates Inc. [3](#), [6](#)
- [2] Jiamu Bai, Xin Yu, Meilong Xu, Weitao Lu, Xin Pan, Kiwan Maeng, Daniel Kifer, Jian Wang, and Yu Wang. Towards better optimization for listwise preference in diffusion models. *arXiv preprint arXiv:2510.01540*, 2025. [2](#)
- [3] Jianrui Cai, Hui Zeng, Hongwei Yong, Zisheng Cao, and Lei Zhang. Toward real-world single image super-resolution: A new benchmark and a new model. In *Proceedings of the IEEE/CVF international conference on computer vision*, pages 3086–3095, 2019. [6](#)
- [4] Bin Chen, Gehui Li, Rongyuan Wu, Xindong Zhang, Jie Chen, Jian Zhang, and Lei Zhang. Adversarial diffusion compression for real-world image super-resolution. In *Proceedings of the IEEE/CVF Conference on Computer Vision and Pattern Recognition*, 2025. [1](#), [2](#)
- [5] Junyang Chen, Jinshan Pan, and Jiangxin Dong. Faithdiff: Unleashing diffusion priors for faithful image super-resolution. In *2025 IEEE/CVF Conference on Computer Vision and Pattern Recognition (CVPR)*, pages 28188–28197, 2025. [1](#), [2](#)
- [6] Zewen Chen, Juan Wang, Wen Wang, Sunhan Xu, Hang Xiong, Yun Zeng, Jian Guo, Shuxun Wang, Chunfeng Yuan, Bing Li, et al. Seagull: No-reference image quality assessment for regions of interest via vision-language instruction tuning. *arXiv preprint arXiv:2411.10161*, 2024. [2](#)
- [7] Qinpeng Cui, Xinyi Zhang, Qiqi Bao, Qingmin Liao, Lu Tian, Zicheng Liu, Zhongdao Wang, Emad Barsoum, et al. Taming diffusion prior for image super-resolution with domain shift sdes. In *The Thirty-eighth Annual Conference on Neural Information Processing Systems*. [1](#), [2](#)
- [8] Chao Dong, Chen Change Loy, Kaiming He, and Xiaoou Tang. Learning a deep convolutional network for image super-resolution. In *Computer Vision – ECCV 2014*, pages 184–199, Cham, 2014. Springer International Publishing. [1](#), [2](#)
- [9] Linwei Dong, Qingnan Fan, Yihong Guo, Zhonghao Wang, Qi Zhang, Jinwei Chen, Yawei Luo, and Changqing Zou. Tsd-sr: One-step diffusion with target score distillation for real-world image super-resolution. In *2025 IEEE/CVF Conference on Computer Vision and Pattern Recognition (CVPR)*, pages 23174–23184, 2025. [1](#), [2](#)
- [10] Zheng-Peng Duan, Jiawei Zhang, Xin Jin, Ziheng Zhang, Zheng Xiong, Dongqing Zou, Jimmy Ren, Chun-Le Guo, and Chongyi Li. Dit4sr: Taming diffusion transformer for real-world image super-resolution. In *Proceedings of the IEEE/CVF International Conference on Computer Vision*, 2025. [3](#), [6](#)
- [11] Jack Hessel, Ari Holtzman, Maxwell Forbes, Ronan Le Bras, and Yejin Choi. CLIPScore: A reference-free evaluation metric for image captioning. In *Proceedings of the 2021 Conference on Empirical Methods in Natural Language Processing*, pages 7514–7528, Online and Punta Cana, Dominican Republic, 2021. Association for Computational Linguistics. [2](#), [3](#)
- [12] Martin Heusel, Hubert Ramsauer, Thomas Unterthiner, Bernhard Nessler, and Sepp Hochreiter. Gans trained by a two time-scale update rule converge to a local nash equilibrium. In *Proceedings of the 31st International Conference on Neural Information Processing Systems*, page 6629–6640, Red Hook, NY, USA, 2017. Curran Associates Inc. [2](#), [3](#)
- [13] Gu Jinjin, Cai Haoming, Chen Haoyu, Ye Xiaoxing, Jimmy S Ren, and Dong Chao. Pipal: a large-scale image quality assessment dataset for perceptual image restoration. In *European conference on computer vision*, pages 633–651. Springer, 2020. [6](#)
- [14] Junjie Ke, Qifei Wang, Yilin Wang, Peyman Milanfar, and Feng Yang. Musiq: Multi-scale image quality transformer. In *2021 IEEE/CVF International Conference on Computer Vision (ICCV)*, pages 5128–5137, 2021. [2](#), [3](#), [6](#)
- [15] Alexander Kirillov, Eric Mintun, Nikhila Ravi, Hanzi Mao, Chloe Rolland, Laura Gustafson, Tete Xiao, Spencer Whitehead, Alexander C Berg, Wan-Yen Lo, et al. Segment anything. In *Proceedings of the IEEE/CVF international conference on computer vision*, pages 4015–4026, 2023. [5](#)
- [16] Yuval Kirstain, Adam Polyak, Uriel Singer, Shahbuland Matiania, Joe Penna, and Omer Levy. Pick-a-pic: an open dataset of user preferences for text-to-image generation. In *Proceedings of the 37th International Conference on Neural Information Processing Systems*, Red Hook, NY, USA, 2023. Curran Associates Inc. [2](#), [3](#)
- [17] Xinqi Lin, Jingwen He, Ziyan Chen, Zhaoyang Lyu, Bo Dai, Fanghua Yu, Yu Qiao, Wanli Ouyang, and Chao Dong. Diffbir: Toward blind image restoration with generative diffusion prior. In *Computer Vision – ECCV 2024: 18th European Conference, Milan, Italy, September 29–October 4, 2024, Proceedings, Part LIX*, page 430–448, Berlin, Heidelberg, 2024. Springer-Verlag. [3](#), [6](#)
- [18] Jie Liu, Gongye Liu, Jiajun Liang, Yangguang Li, Jiaheng Liu, Xintao Wang, Pengfei Wan, Di Zhang, and Wanli Ouyang. Flow-grpo: Training flow matching models via online rl. *arXiv preprint arXiv:2505.05470*, 2025. [2](#)
- [19] William Peebles and Saining Xie. Scalable diffusion models with transformers. In *2023 IEEE/CVF International Conference on Computer Vision (ICCV)*, pages 4172–4182, 2023. [3](#)
- [20] Chitwan Saharia, Jonathan Ho, William Chan, Tim Salimans, David J. Fleet, and Mohammad Norouzi. Image super-resolution via iterative refinement. *IEEE Transactions on Pattern Analysis and Machine Intelligence*, 45(4):4713–4726, 2023. [1](#), [2](#)

[21] Christoph Schuhmann, Romain Beaumont, Richard Vencu, Cade Gordon, Ross Wightman, Mehdi Cherti, Theo Coombes, Aarush Katta, Clayton Mullis, Mitchell Wortsman, Patrick Schramowski, Srivatsa Kundurthy, Katherine Crowson, Ludwig Schmidt, Robert Kaczmarczyk, and Jenia Jitsev. Laion-5b: an open large-scale dataset for training next generation image-text models. In *Proceedings of the 36th International Conference on Neural Information Processing Systems*, Red Hook, NY, USA, 2022. Curran Associates Inc. [2](#), [3](#)

[22] Oriane Siméoni, Huy V Vo, Maximilian Seitzer, Federico Baldassarre, Maxime Oquab, Cijo Jose, Vasil Khalidov, Marc Szafraniec, Seungeun Yi, Michaël Ramamonjisoa, et al. Dinov3. *arXiv preprint arXiv:2508.10104*, 2025. [5](#)

[23] Chenyue Song, Chen Hui, Haiqi Zhu, Feng Jiang, Yachun Mi, Wei Zhang, and Shaohui Liu. Segmenting and understanding: Region-aware semantic attention for fine-grained image quality assessment with large language models. *arXiv preprint arXiv:2508.07818*, 2025. [2](#)

[24] Haoze Sun, Wenbo Li, Jianzhuang Liu, Haoyu Chen, Renjing Pei, Xueyi Zou, Youliang Yan, and Yujiu Yang. Coser: Bridging image and language for cognitive super-resolution. In *2024 IEEE/CVF Conference on Computer Vision and Pattern Recognition (CVPR)*, pages 25868–25878, 2024. [3](#)

[25] Lingchen Sun, Rongyuan Wu, Zhiyuan Ma, Shuaizheng Liu, Qiaosi Yi, and Lei Zhang. Pixel-level and semantic-level adjustable super-resolution: A dual-lora approach. 2025. [3](#)

[26] Bram Wallace, Meihua Dang, Rafael Rafailov, Linqi Zhou, Aaron Lou, Senthil Purushwalkam, Stefano Ermon, Caiming Xiong, Shafiq Joty, and Nikhil Naik. Diffusion model alignment using direct preference optimization. In *Proceedings of the IEEE/CVF Conference on Computer Vision and Pattern Recognition*, pages 8228–8238, 2024. [2](#), [6](#), [8](#)

[27] Jianyi Wang, Kelvin CK Chan, and Chen Change Loy. Exploring clip for assessing the look and feel of images. In *Proceedings of the AAAI conference on artificial intelligence*, pages 2555–2563, 2023. [2](#), [3](#), [6](#)

[28] Jianyi Wang, Zongsheng Yue, Shangchen Zhou, Kelvin C.K. Chan, and Chen Change Loy. Exploiting diffusion prior for real-world image super-resolution. 2024. [2](#)

[29] Xintao Wang, Liangbin Xie, Chao Dong, and Ying Shan. Real-esrgan: Training real-world blind super-resolution with pure synthetic data. In *2021 IEEE/CVF International Conference on Computer Vision Workshops (ICCVW)*, pages 1905–1914, 2021. [1](#), [2](#), [4](#)

[30] Yufei Wang, Wenhan Yang, Xinyuan Chen, Yaohui Wang, Lanqing Guo, Lap-Pui Chau, Ziwei Liu, Yu Qiao, Alex C Kot, and Bihan Wen. Sinsr: diffusion-based image super-resolution in a single step. In *Proceedings of the IEEE/CVF Conference on Computer Vision and Pattern Recognition*, pages 25796–25805, 2024. [1](#), [2](#)

[31] Zhou Wang, A.C. Bovik, H.R. Sheikh, and E.P. Simoncelli. Image quality assessment: from error visibility to structural similarity. *IEEE Transactions on Image Processing*, 13(4): 600–612, 2004. [3](#), [6](#)

[32] Pengxu Wei, Ziwei Xie, Hannan Lu, Zongyuan Zhan, Qixiang Ye, Wangmeng Zuo, and Liang Lin. Component divide-and-conquer for real-world image super-resolution. In *European conference on computer vision*, pages 101–117. Springer, 2020. [6](#)

[33] Rongyuan Wu, Lingchen Sun, Zhiyuan Ma, and Lei Zhang. One-step effective diffusion network for real-world image super-resolution. *Advances in Neural Information Processing Systems*, 37:92529–92553, 2024. [1](#), [2](#)

[34] Rongyuan Wu, Tao Yang, Lingchen Sun, Zhengqiang Zhang, Shuai Li, and Lei Zhang. Seesr: Towards semantics-aware real-world image super-resolution. In *Proceedings of the IEEE/CVF conference on computer vision and pattern recognition*, pages 25456–25467, 2024. [3](#), [6](#)

[35] Xiaoshi Wu, Yiming Hao, Keqiang Sun, Yixiong Chen, Feng Zhu, Rui Zhao, and Hongsheng Li. Human preference score v2: A solid benchmark for evaluating human preferences of text-to-image synthesis. *arXiv preprint arXiv:2306.09341*, 2023. [2](#), [3](#)

[36] Jiazheng Xu, Xiao Liu, Yuchen Wu, Yuxuan Tong, Qinkai Li, Ming Ding, Jie Tang, and Yuxiao Dong. Imagereward: learning and evaluating human preferences for text-to-image generation. In *Proceedings of the 37th International Conference on Neural Information Processing Systems*, pages 15903–15935, 2023. [2](#), [3](#), [6](#), [7](#), [8](#)

[37] Zeyue Xue, Jie Wu, Yu Gao, Fangyuan Kong, Lingting Zhu, Mengzhao Chen, Zhiheng Liu, Wei Liu, Qiushan Guo, Weilin Huang, et al. Dancegrpo: Unleashing grpo on visual generation. *arXiv preprint arXiv:2505.07818*, 2025. [2](#), [6](#), [8](#)

[38] Sidi Yang, Tianhe Wu, Shuwei Shi, Shanshan Lao, Yuan Gong, Mingdeng Cao, Jiahao Wang, and Yujiu Yang. Maniqa: Multi-dimension attention network for no-reference image quality assessment. In *Proceedings of the IEEE/CVF Conference on Computer Vision and Pattern Recognition*, pages 1191–1200, 2022. [2](#), [3](#), [6](#)

[39] Tao Yang, Rongyuan Wu, Peiran Ren, Xuansong Xie, and Lei Zhang. Pixel-aware stable diffusion for realistic image super-resolution and personalized stylization. In *European conference on computer vision*, pages 74–91. Springer, 2024. [3](#)

[40] Fanghua Yu, Jinjin Gu, Zheyuan Li, Jinfan Hu, Xiangtao Kong, Xintao Wang, Jingwen He, Yu Qiao, and Chao Dong. Scaling up to excellence: Practicing model scaling for photo-realistic image restoration in the wild. In *2024 IEEE/CVF Conference on Computer Vision and Pattern Recognition (CVPR)*, pages 25669–25680, 2024. [3](#)

[41] Fanghua Yu, Jinjin Gu, Zheyuan Li, Jinfan Hu, Xiangtao Kong, Xintao Wang, Jingwen He, Yu Qiao, and Chao Dong. Scaling up to excellence: Practicing model scaling for photo-realistic image restoration in the wild. In *Proceedings of the IEEE/CVF conference on computer vision and pattern recognition*, pages 25669–25680, 2024. [6](#)

[42] Zongsheng Yue, Jianyi Wang, and Chen Change Loy. Resshift: efficient diffusion model for image super-resolution by residual shifting. In *Proceedings of the 37th International Conference on Neural Information Processing Systems*, Red Hook, NY, USA, 2023. Curran Associates Inc. [1](#), [2](#)

[43] Zongsheng Yue, Kang Liao, and Chen Change Loy. Arbitrary-steps image super-resolution via diffusion inver

sion. In *2025 IEEE/CVF Conference on Computer Vision and Pattern Recognition (CVPR)*, pages 23153–23163, 2025. [1](#), [2](#)

[44] Kai Zhang, Jingyun Liang, Luc Van Gool, and Radu Timofte. Designing a practical degradation model for deep blind image super-resolution. In *IEEE International Conference on Computer Vision*, pages 4791–4800, 2021. [1](#), [2](#)

[45] Lvmin Zhang, Anyi Rao, and Maneesh Agrawala. Adding conditional control to text-to-image diffusion models, 2023. [3](#)

[46] Leheng Zhang, Weiyi You, Kexuan Shi, and Shuhang Gu. Uncertainty-guided perturbation for image super-resolution diffusion model. In *2025 IEEE/CVF Conference on Computer Vision and Pattern Recognition (CVPR)*, pages 17980–17989, 2025. [1](#), [2](#)

[47] Richard Zhang, Phillip Isola, Alexei A. Efros, Eli Shechtman, and Oliver Wang. The unreasonable effectiveness of deep features as a perceptual metric. In *2018 IEEE/CVF Conference on Computer Vision and Pattern Recognition*, pages 586–595, 2018. [3](#)

[48] Richard Zhang, Phillip Isola, Alexei A Efros, Eli Shechtman, and Oliver Wang. The unreasonable effectiveness of deep features as a perceptual metric. In *Proceedings of the IEEE conference on computer vision and pattern recognition*, pages 586–595, 2018. [6](#)

[49] Sixian Zhang, Bohan Wang, Junqiang Wu, Yan Li, Tingting Gao, Di Zhang, and Zhongyuan Wang. Learning multi-dimensional human preference for text-to-image generation. In *Proceedings of the IEEE/CVF Conference on Computer Vision and Pattern Recognition*, pages 8018–8027, 2024. [2](#), [3](#)

[50] Weixia Zhang, Guangtao Zhai, Ying Wei, Xiaokang Yang, and Kede Ma. Blind image quality assessment via vision-language correspondence: A multitask learning perspective. In *IEEE Conference on Computer Vision and Pattern Recognition*, pages 14071–14081, 2023. [2](#), [3](#), [6](#)

[51] Yulun Zhang, Kunpeng Li, Kai Li, Lichen Wang, Bineng Zhong, and Yun Fu. Image super-resolution using very deep residual channel attention networks. In *ECCV*, 2018. [1](#), [2](#)